THE JOURNAL OF PHYSICAL CHEMISTRY B

Article

pubs.acs.org/JPCB

Self-Assembly of Block Copolymer Chains To Promote the Dispersion of Nanoparticles in Polymer Nanocomposites

Jun Liu,[†] Zixuan Wang,[†] Zhiyu Zhang,[†] Jianxiang Shen,[‡] Yulong Chen,[§] Zijian Zheng,*[,†,∥] Liqun Zhang,*[,†] and Alexey V. Lyulin*[,⊥]

[†]Key Laboratory of Beijing City on Preparation and Processing of Novel Polymer Materials, Beijing University of Chemical Technology, Beijing 100029, P. R. China

[∥]Hubei Collaborative Innovation Center for Advanced Organic Chemical Materials, Key Laboratory for the Green Preparation and Application of Functional Materials, Ministry of Education, Hubei Key Laboratory of Polymer Materials, School of Materials Science and Engineering, Hubei University, Wuhan 430062, P. R. China

[‡]College of Materials and Textile Engineering, Jiaxing University, Jiaxing 314001, P. R. China

[§]College of Material Science and Engineering, Zhejiang University of Technology, Hangzhou 310014, P. R. China

[⊥]Theory of Polymers and Soft Matter, Department of Applied Physics Technische Universiteit Eindhoven, 5600 MB Eindhoven, The Netherlands

S *Supporting Information*

ABSTRACT: In this paper we adopt molecular dynamics simulations to study the amphiphilic AB block copolymer (BCP) mediated nanoparticle (NP) dispersion in polymer nanocomposites (PNCs), with the A-block being compatible with the NPs and the B-block being miscible with the polymer matrix. The effects of the number and components of BCP, as well as the interaction strength between A-block and NPs on the spatial organization of NPs, are explored. We find that the increase of the fraction of the A-block brings different dispersion effect to NPs than that of B-block. We also find that the best dispersion state of the NPs occurs in the case of a moderate interaction strength between the A-block and the NPs. Meanwhile, the stress−strain behavior is probed. Our simulation results verify that adopting BCP is an effective way to adjust the dispersion of NPs in the polymer matrix, further to manipulate the mechanical properties.

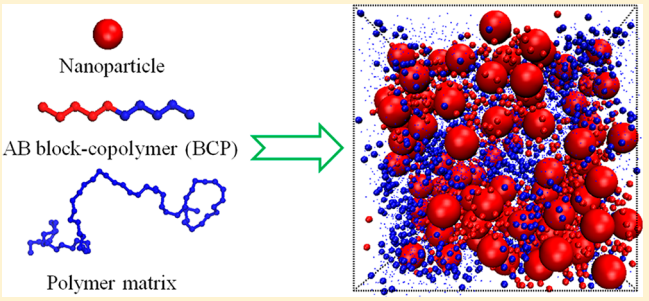

1. INTRODUCTION

Polymers are inexpensive and easy to process, while nanoscale additives are widely used to introduce additional functionalities to, or improve the mechanical,[1−8] electrical[9−12] and optical properties[13−16] of, polymer matrices. It is well established that the state of the dispersion of nanofillers is crucial to the properties of polymer nanocomposites (PNCs), and, thus, there has been considerable interest in controllably dispersing nanofillers into polymer matrices,[4,17−30] with the obvious goal of optimizing the macroscopic properties of the resulting polymer PNCs. In achieving these property enhancements, it is critical to control the spatial arrangement of the nanofillers in the polymer host. One popular strategy is to evenly or homogeneously graft the nanoparticle (NP) surfaces with the end-functionalized polymer chains, which have the same chemical structure as the polymer matrix. However, this is rather uncontrollable, time-consuming, and a costly approach, and thus it is practically unlikely to be utilized on a large industrial scale.

The easiest and most applicable approach relies on introducing attractive interactions between the functionalized block of the copolymer chains and the surface of nanofillers, to effectively prevent them from a large-scale aggregation.[31−35] Block copolymer (BCP) nanocomposites have received substantial attention due to the long-range order of the corresponding matrix.[36,37] A large amount of research has focused on grafting BCP short chains onto the surface of NPs by generating chemical bonding.[37−44] In contrast to that, the cases in which BCP chains are physically attracted onto the surface of nanofillers, while the other end of BCP chain is kept chemically identical to the polymer matrix chains for a better dispersion, have not been studied in sufficient detail.

Based on the work of Kumar et al.,[37] a model of PNCs filled with block copolymer short chains is introduced here. Kumar et al.[37] experimentally mixed silica NPs into the polystyrene (PS) matrix, and then filled the resulting PNC with short PSbP2VP BCP chains, with the polar poly(2-vinylpyridine) (P2VP) on one end. The hydrogen bonding between the surface silanol

Received: August 31, 2017
Revised: September 11, 2017
Published: September 11, 2017

DOI: 10.1021/acs.jpcb.7b08670
J. Phys. Chem. B 2017, 121, 9311−9318

groups and the nitrogen on the P2VP enabled the physical adsorption of this block copolymer with a NP-philic ("P") and a NP-phobic ("H") block. This, in turn, leads to a better control of the NP dispersion state.

In the present study, we explore the dispersion state of the NPs in the polymer matrix, by introducing the block copolymer chains with various chemical and physical characteristics. Different from the work of Kumar et al.,[37] here we focus mainly on studying the dispersion mechanism by systematically tuning a large library of the structural parameters through the coarse-grained molecular dynamics (MD) simulations. Meanwhile, the tensile strength of the polymer nanocomposite made of the BCPs physically adsorbed onto the nanofillers is investigated at different dispersion states. Our results could provide a systematically effective approach to manipulate the spatial distribution of NPs in the polymer matrix, by employing the physically adsorbed block copolymer chains as the surface modifiers of the nanofillers.

2. MODEL AND SIMULATION METHOD

2.1. Model and the Implemented Force Field. Here we adopt the classical bead−spring coarse-grained model to simulate both matrix polymer chains and the block copolymer chains. In the model each bead corresponds to 3−6 covalent bonds in a realistic polymer chain. In the present simulations four types of the Lennard-Jones (LJ) beads have been used, as listed in Table 1.

Table 1. Parameters of the Simulated Beads in a Coarse-Grained Model

atom type	representation	bead diameter	bead mass
1	A-block of BCP	1	1
2	B-block of BCP	1	1
3	matrix polymer chain	1	1

Each matrix polymer chain in the simulation box consists of 60 beads, for the purpose of making the mean-squared end-to-end distance of polymer chains comparable with the diameter of NPs. While we utilize rather short matrix chains, they show the static and dynamic characteristics of realistic polymers. In the present simulations the number and the length of matrix polymer chains are fixed.

The block copolymer chains are constructed as shown in Figure 1. The BCP chain length is varied from 10 to 30 beads. The number of BCP chains is determined by the average density Σ of BCP chains per NP,

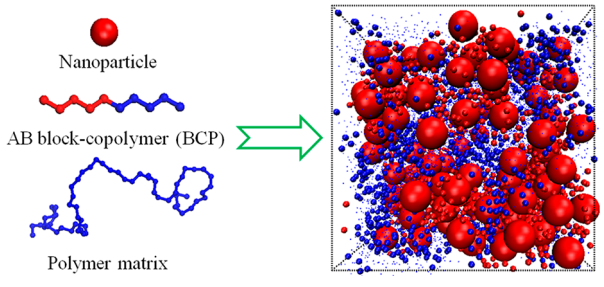

Figure 1. Schematics of NPs, BCPs, and a polymer matrix. Elements with the same color denote attractive interactions, while the elements with different colors repel each other.

$$\Sigma = \frac{N_b}{4\pi R_{NP}^2} \quad (1)$$

where N_b is the number of BCP chains to be averagely adsorbed onto each NP with radius R_{NP}. As the diameter of each matrix chain bead is set to $\sigma = 1.0$, a density of, for example, $\Sigma = 0.48$ means approximately 24 chains adsorbed onto each NP surface; see more in the Table 2.

Table 2. Simulated Densities and the Corresponding Number N_b of Block Copolymer Chains

average density Σ of BCP per NP	0.04	0.08	0.16	0.32	0.48
no. N_b of BCP chains	200	400	800	1200	2400

In our simulation, we set the diameter of each nanoparticle to be four times the diameter of each matrix chain bead. The nonbonded interactions are modeled by the expanded truncated and shifted Lennard-Jones (LJ) potential. These nonbonded interactions include NP−NP, NP−polymer, and polymer−polymer interactions and are given by

$$U = \begin{cases} 4\varepsilon\left[\left(\frac{\sigma}{r-\Delta}\right)^{12} - \left(\frac{\sigma}{r-\Delta}\right)^{6}\right] & r < r_{cutoff} + \Delta \\ 0 & r \geq r_{cutoff} + \Delta \end{cases} \quad (2)$$

where ε is the pair interaction energy parameter, r is the distance between two interaction sites, σ is the characteristic size, and Δ is introduced to take into account the effect of the excluded volume of different interaction sites. The LJ potential (eq 2) is cut off at different distances to model the attractive ($r_{cutoff} = 2.5\sigma$) as well as repulsive ($r_{cutoff} = 1.12\sigma$) interactions. The r_{cutoff} stands for the cutoff distance at which the interaction is truncated and shifted so that the energy is equal to zero. The LJ parameters for all types of interactions are listed in Table S1. Since it is not our purpose to study any chemically specific polymer, the force-field parameters σ, ε, and m are all set to unity, and all the simulated parameters are dimensionless. The bonded interactions between the neighbor beads along a polymer chain are modeled using the harmonic potential,

$$E_{bond} = k(r - r_0)^2 \quad (3)$$

where $k = 500.0$ and $r = 1.0$, ensuring a certain stiffness while preventing the polymer beads from becoming overlapped with each other.

2.2. Equilibration Procedure. To generate equilibrated configurations, initially all the matrix polymer chains and block copolymer chains together with NPs have been placed in a rather large simulation box. Such structures are further equilibrated under the NPT ensemble with $T^* = 1.0$ above the glass transition temperature ($T = 0.41$) by using the Nose−Hoover thermostat and barostat. The selection of pressure yields an equilibrium number density of the polymer beads around $\rho^* = 0.85$, corresponding to the realistic density of typical polymer melts.[45] Periodic boundary conditions are applied in all three directions. The velocity Verlet algorithm is used to integrate the equations of motion, with a time step $\delta t = 0.001\tau$ (in LJ time $\tau = \sigma\sqrt{\frac{m}{\varepsilon}}$ units).

The obtained structures are further equilibrated under the NVT ensemble with $T = 1.0$ over a long time. To obtain well-equilibrated samples, the total equilibration time is accordingly increased for the larger systems. After the equilibration of the

DOI: 10.1021/acs.jpcb.7b08670
J. Phys. Chem. B 2017, 121, 9311−9318

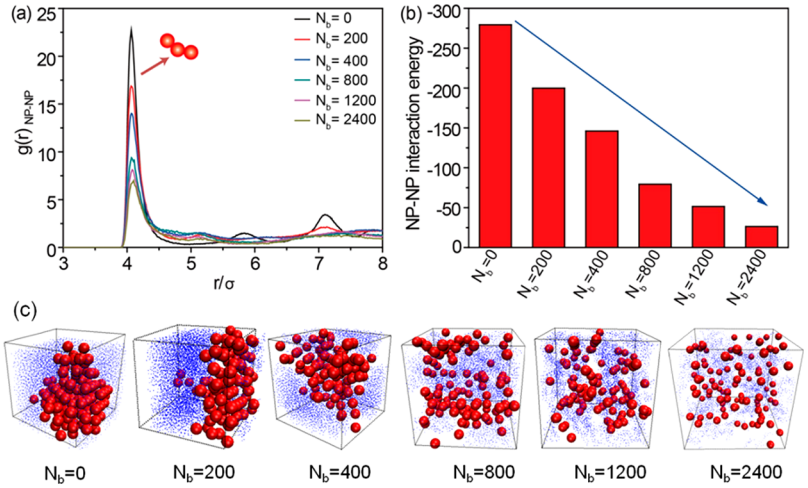

Figure 2. (a) The radial distribution functions $g(r)$ of the NPs for various densities of BCPs. (b) The total NP−NP interaction energy for various densities of BCPs. (c) The snapshots of the simulation systems for various densities of BCPs. For clarity, only the red spheres representing NPs and blue dots representing the matrix beads are shown. The length of BCP chains equals 10 polymer beads.

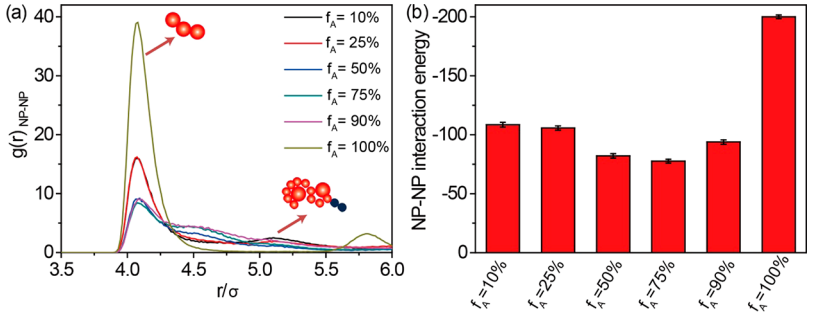

Figure 3. (a) The radial distribution functions $g(r)$ of the NPs for the variation of the fraction of the A-block. (b) The total NP−NP interaction energy for the BCPs with variation of the fraction of the A-block. The length of BCP chains equals 20 polymer beads.

system at least for 5×10^7 MD steps, the structural and dynamic data were collected for further analysis. The change of the potential energy is plotted in Figure S1a. Meanwhile, the change of the mean square end-to-end distance R_{end}^2 and radius of gyration R_g^2 are presented in Figure S1b. Obviously, they exhibit small fluctuations, which verify that our simulated systems have been fully and properly equilibrated.

2.3. Nonequilibrium Simulations. We hereby implement the SLLOD equations of motion,[46] the widely used method for the nonequilibrium molecular dynamics study of the tensile deformation. The length L_y of the simulation box in the Y-direction has been increased at a fixed engineering strain, while the box lengths in the X- and Z-directions are contracted simultaneously to maintain the constant volume of the simulation box during the deformation process. The other approach is the triaxial deformation to induce the failure, namely, the simulation box is extended in one direction, while the other two dimensions are held fixed, which results in a positive effective stress in all directions.[47,48] The tensile strain rate is defined as

$$\dot{\varepsilon} = \frac{L_y(t) - L_y(0)}{L_y(0)} = 0.0327/\tau \tag{4}$$

which is the same as the simulation work from Gao et al.[49,50] The average tensile stress σ_t is calculated from the corresponding component of the stress tensor as

$$\sigma_t = (1 + \mu)(-P_{yy} + P) \approx 3(-P_{yy} + P)/2 \tag{5}$$

Here $P = \sum_i (P_{ii}/3)$ is the imposed isotropic pressure. The parameter μ is the Poisson ratio, which is equal to 0.5 in the present simulations.

All MD runs are carried out using the Large-scale Atomic/Molecular Massively Parallel Simulator (LAMMPS) developed by Sandia National Laboratories.[51] More simulation details can be found in our previous work.[52−54]

3. RESULTS AND DISCUSSION

3.1. The Effects of Number and Component of the Block Copolymer. In order to explore the dispersion and the spatial distribution of the bare NPs in polymer melts filled with the block copolymer short chains, we first change the number of BCP chains (L_b) while keeping the other parameters unchanged. The length of BCP chains has been fixed at 10 polymer beads. The radial distribution functions (RDF) of the NPs have been calculated to characterize the nanoparticle dispersion state, as shown in Figure 2a. The highest peak at $r = 4.0\sigma$ has been clearly observed for all the simulation systems, indicating a nearly direct contact of NPs. Obviously, the peak at $r = 4.0\sigma$ decreases once the BCP chains are added into the system. As the number of BCP chains increases, the peak at $r = 4.0\sigma$ gradually decreases, displaying that we can adopt more BCP chains to improve the NP dispersion state. To quantitatively characterize the filler dispersion state as a function of BCP chains, the total NP−NP interaction energy

DOI: 10.1021/acs.jpcb.7b08670
J. Phys. Chem. B 2017, 121, 9311−9318

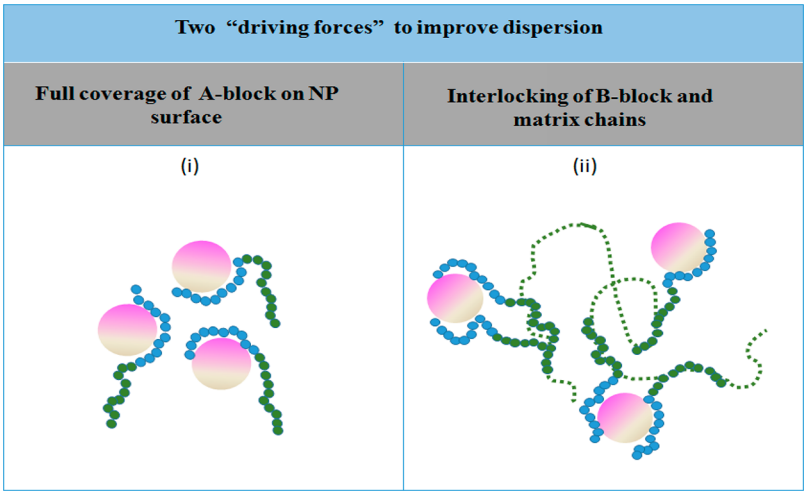

Figure 4. Two different mechanisms to improve the dispersion state of NPs in nanocomposites filled with BCP chains.

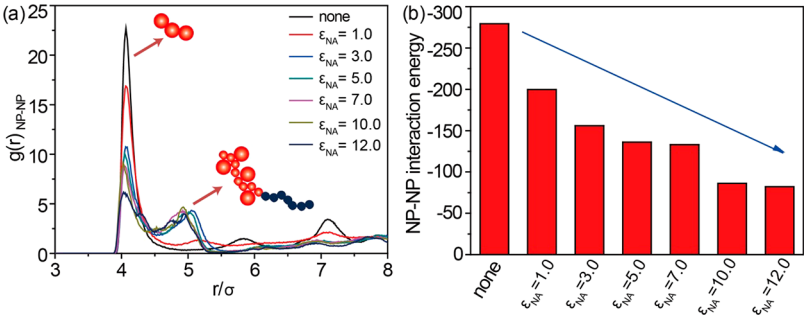

Figure 5. (a) The radial distribution functions $g(r)$ of the NPs for the variation of the interaction strength ε_{NA} between NPs and the A-block of the block copolymer. (b) The total NP−NP interaction energy as a function of interaction strength ε_{NA} between the nanoparticle and the A-block of the block copolymer. Note that the average density of BCP per NP equals 0.04.

is calculated, as displayed in Figure 2b. Evidently, the smaller the absolute value of NP−NP interaction energy, the better the dispersion state of the NPs. In line with the conclusion of RDF, the NPs disperse well with the increasing numbers of BCP chains. Snapshots corresponding to the different numbers of BCP chains are also shown in Figure 2c. Obviously, the NPs aggregate severely in the system without BCP chains. The dispersion state shifts from aggregate state to dispersion state with increasing number of BCP chains; a relatively good dispersion is seen for N_b = 2400. We further investigate the effect of BCP chain length on the dispersion state of NPs. Note that we adopt different numbers of BCP chains to guarantee that the total number of A beads is the same for these three systems. For example, at the length of L_b = 10, there exist 1200 BCP chains; at the length of L_b = 30, there exist 400 BCP chains. We also use the RDF of NPs and total NP−NP interaction energy to display the dispersion state of NPs, as shown in Figure S2. Clearly, the NPs disperse well in short BCP chains, attributed to the fact that the A-block of short BCP chains can diffuse easily onto the surface of the NPs, and the "thickness" formed by A-block around each NP is large with short BCP chains.

We then explore how the fraction of the A-block can affect the dispersion state of NPs by adopting six different values, 10%, 25%, 50%, 75%, 90%, and keeping the length of BCP chains fixed at 20 polymer beads. We again have calculated the RDF of NPs, as is shown in Figure 3a. It is seen that as A-block becomes more and more dominant, the peak at $r = 4.0\sigma$ first decreases and then increases. This observation implies that a good dispersion can be obtained at a fraction of the A-block. To clarify this even better, we monitor the NP−NP interaction energy as a function of the fraction of the A-block, see Figure 3b. Obviously, the absolute value of NP−NP interaction energy remains the lowest for the 75% fraction of the A-block, suggesting the best dispersion state. We explain the above phenomenon as follows: On the one hand, the longer A-block chains can cover the surface of the NPs thoroughly, initially keeping NPs separated from each other, and thus driving the dispersion of NPs. On the other hand, the longer B-block chains can result in the interlocking between the B-blocks and the matrix polymer chains, inducing more matrix polymer chains into the surface of NPs to drive the dispersion of NPs. These two mechanisms compete with each other, thus resulting in there existing a best fraction of the A-block.

We then suggest that there exist two major "driving forces" for the dispersion process: (i) the coverage and shielding of the A-block onto the surface of NPs; (ii) the pulling and drawing caused by the interlocking of the B-block and the matrix polymer chains. See Figure 4 for the illustration. This mechanism was also suggested recently by Ferrier et al.[16] Their analytical calculations show that gold nanorods can achieve better dispersion when filled with bifunctional gold nanorods (B-NRs). They also show that the short chains force the matrix chains to come together and, therefore, promote wetting by the matrix chains.

DOI: 10.1021/acs.jpcb.7b08670
J. Phys. Chem. B 2017, 121, 9311−9318

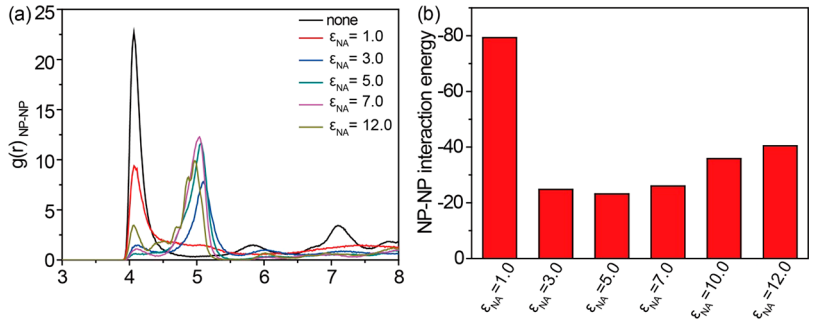

Figure 6. (a) The radial distribution functions $g(r)$ of the NPs for the variation of the interaction strength ε_{NA} between NPs and the A-block of the block copolymer. (b) The total NP−NP interaction energy as a function of interaction strength ε_{NA} between the nanoparticle and the A-block of the block copolymer. Note that the average density of BCP per NP equals 0.16.

On the basis of the above simulated results, it is concluded that we can tune the number of BCP chains to adjust the dispersion behavior of NPs. The more BCP chains, the better the dispersion state. Meanwhile, at the same total number of A beads, the short BCP chain can be propitious to the dispersion of NPs. Moreover, there exists a moderate fraction of A-block in acquiring a better dispersion state. However, the RDF of NPs of all of the above simulation systems have a peak at $r = 4.0\sigma$, showing that there exists direct contact of NPs.

3.2. Effect of the Interaction Strength between NPs and A-Block. In the work of Jouault et al.,[37] the silica NPs with the polystyrene-*b*-poly(2-vinylpyridine) (PSbP2VP) in various polystyrene (PS) matrices have been physically blended, employing the hydrogen bonding between the surface silanol groups and the nitrogen on the P2VP to form a polymer shell on the surface of NPs, driving the dispersion of NPs. Clearly, the interaction energy between A-block and NPs is vital for the dispersion of NPs. It is clear that it is difficult to tune the interactions between P2VP and silica in the actual experiment, while it is quite convenient in the MD simulation. Here, we explore the effect of the A-block−NP interaction energy (ε_{NA}) on the dispersion of NPs, as shown in Figure 5. We adopt a range of the interaction energies between A-block and NPs, varying from $\varepsilon_{NA} = 1.0$ to $\varepsilon_{NA} = 12.0$, while keeping the number of BCP fixed at 200, corresponding to the average density of BCP per NP ($\Sigma = 0.04$). It should be noted that, when mapping the bead−spring model to real polymers, the energy parameter ε is about 2.5−4.2 kJ/mol for different polymers,[45] indicating that the value of 12 (in units of ε) for the NP−A-block interactions is about 30−50 kJ/mol. The reported interaction strengths of saturated hydrocarbon elastomers with the adsorption sites on the silica surfaces can vary from 27 to 35 kJ/mol, which are mainly due to van der Waals forces.[55] In fact, the functional groups in many kinds of polymers (such as PVA and PDMS) can form hydrogen bonds with the functional groups on the NPs' surface, which make the interfacial strengths stronger. Thus, the interaction of $\varepsilon_{NA} = 12.0$ adopted in our simulations is higher than that between the saturated hydrocarbon elastomers and NP and is more appropriate to mimic the strong NP−polymer attractions (such as hydrogen bonds) in real nanocomposite systems.

From the RDF of NP−A-block, we can obtain that the peak at about $r = 2.5\sigma$ increases with the increase of ε_{NA}, demonstrating that the A-blocks are forced to absorb around the surface of NPs, as shown in Figure S3. We calculate the RDF of NPs to reflect the dispersion behavior in Figure 5a, showing that the direct contact aggregation of NP degree decreases with an increase of ε_{NA}. The NPs tend to form aggregates sandwiched by one polymer layer if the ε_{NA} is greater than or equal to 3.0, which is reflected by the peaks located at $r = 5.0\sigma$. We can obtain the conclusion that, in low average density of BCP per NP, the higher ε_{NA}, the better the dispersion state. The total NP−NP interaction energy further verifies this conclusion, as illustrated in Figure 5b. However, even when $\varepsilon_{NA} = 12.0$, there still exists a direct contact peak of NPs at $r = 4.0\sigma$.

We further investigate the effect of ε_{NA} on the dispersion behavior of NPs in a higher average density of BCP per NP ($\Sigma = 0.16$). Similar to the low average density, the A-blocks are gradually absorbed around the surface of NPs with an increase of ε_{NA}, as displayed in Figure S4. However, the RDF of NPs in Figure 6a shows that only small peaks appear without direct contact aggregation of the NPs when $\varepsilon_{NA} = 5.0$. This observation implies that a good dispersion can be obtained at a moderate ε_{NA}. The total NP−NP interaction energy can further support this conclusion, as shown in Figure 6b. This simulated result is very similar to some theoretical predictions.[29]

Using the above analysis, we could speculate about the reason why this moderate interaction energy occurs for the dispersion of the NPs. The spatial arrangement of one BCP chain around one NP is illustrated in Figure 7. At low ε_{NA}, the

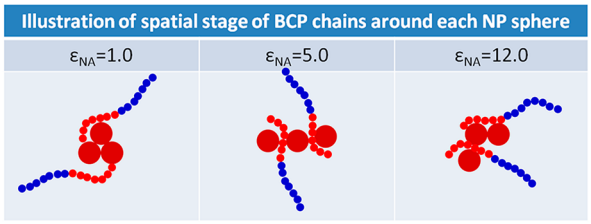

Figure 7. Illustration of the spatial state of the BCP chains around each NP subtracted from a system of BCP-filled nanocomposites with the change of the parameter ε_{NA}.

BCP chain and the NP are initially rather far apart, leaving sufficient free surface for other NPs to approach and thus aggregate. With ε_{NA} becoming larger, the BCP comes closer to the NP surface, but still being maintained at a moderate distance, covering the surface so that neighboring NPs are not able to contact directly with each other. With the further increase of ε_{NA}, the BCP chain comes adjacent to the surface of NP that another NP attracts onto the surface of BCP polymer beads, forming a sandwich structure. This sandwich structure

DOI: 10.1021/acs.jpcb.7b08670
J. Phys. Chem. B 2017, 121, 9311−9318

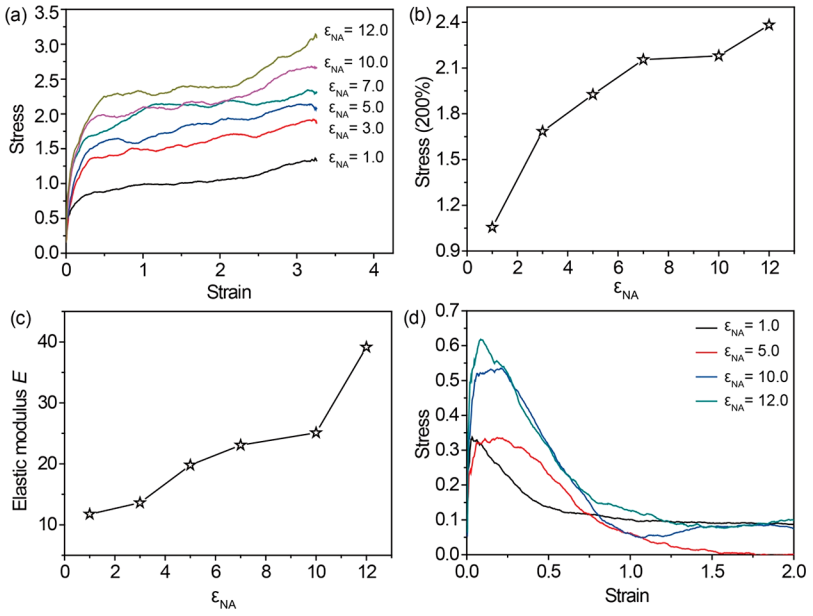

Figure 8. (a) The stress−strain behavior for various dispersion states of NPs by changing the interaction strength ε_{NA} between NPs and the A-block of the block copolymer. (b) The stress of the above systems at the strain equal to 200%. (c) The elastic modulus of the above systems. (d) The stress required to break the above systems.

contributes to another kind of NP aggregate bridged by the BCP polymer chains.

Based on the above results, it is clear the dispersion state of NPs mainly depends on the interaction energy ε_{NA} at low BCP content. In other words, the higher ε_{NA} (such as hydrogen bonds), the better the dispersion state, while at high BCP content, there exists a moderate interaction energy ε_{NA} (about 5.0).

3.3. Stress−Strain Behavior of BCP-Filled PNCs. Finally, we study the tensile process of PNCs at different dispersion states through changing the interaction energy between the BCP polymer chains and NPs. We mainly adopt two different approaches. The first approach is stretching the simulation box along the *Y*-direction while keeping the box volume constant to acquire the stress−strain behavior. The other approach is stretching the simulation box along the *Y*-direction while keeping the box length at *X*-direction and *Z*-direction constant to acquire the stress required to break. Figure 8a displays the stress−strain characteristics corresponding to the various ε_{NA}. It is evident that as ε_{NA} becomes larger, the tensile stress is progressively enhanced, indicating that the dispersion state of NPs has been improved, which was discussed in our previous work.[56] The simulated temperature is set to T = 1.0, which is higher than the corresponding T_g about T = 0.41.[45] For a better quantitative analysis, we examine the degree of mechanical reinforcement by comparing the tensile stress at the 200% strain, as shown in Figure 8b. Again, it confirms further a rising tendency of the tensile stress. Moreover, we compute the elastic modulus of the nanocomposites at different levels of NP dispersion form the stress−strain behavior at small strain (ranging from 0% to 3%), as shown in Figure 8c. Similar to the above results, the elastic modulus increased gradually as the dispersion state became better. Lastly, we calculate the stress required to break the PNCs at different dispersion states, as displayed in Figure 8d. Evidently, at small strain the polymer chains respond elastically, and then a well-defined yielding point is observed, whose position seems to be independent of ε_{NA}. The yielding stress indicates that the mechanical properties of PNCs are at a high level when the NPs disperse well. In all, our simulation results indicate that the physical absorption of short BCP chains onto the surface of NPs is a relatively effective way of dispersing NPs, and further to enhance the mechanical properties of the corresponding PNCs, given the fact that the chemical grafting process in large-scale industrial applications could be rather expensive.

4. CONCLUSIONS

Detailed coarse-grained MD simulations have been carried out to systematically explore the effects of the number, length, and components of the block copolymer modifier, the interaction strength between nanofillers, and the interaction strength between nanofillers and the A-block of the block copolymer chain, on the dispersion of spherical NPs in the polymer matrix. The results indicate that there exist two major "driving forces" for the dispersion process: (i) the coverage of the A-block onto the surface of NPs and (ii) the pulling and drawing caused by the interlocking of the B-block and the polymer matrix chains. Interestingly, we find that, at low average density of BCP per NP (Σ = 0.04), the dispersion state of NPs mainly depends on the interaction energy between A-block and NPs, while at high average density (Σ = 0.16) there exists a moderate interaction strength between the A-block and the NP for the best dispersion of the nanofillers, which is attributed to the three different states of the filler spatial organization as a function of this interaction strength. By comparing the stress−strain behavior of the nanocomposite with block copolymer chains physically and chemically adsorbed onto the filler nanoparticles, we find that their mechanical properties are very comparable. Generally, these systematical investigations of the dispersion BCP-mediated nanoparticles with various shapes can assist in the rational design of high performance polymer nanocomposite materials.

DOI: 10.1021/acs.jpcb.7b08670
J. Phys. Chem. B 2017, 121, 9311−9318

■ ASSOCIATED CONTENT

Supporting Information

The Supporting Information is available free of charge on the ACS Publications website at DOI: 10.1021/acs.jpcb.7b08670.

Plots of potential energy, R_{end}^2, and R_g^2 vs MD steps, parameters of Lennard-Jones interactions, and radial distribution plots (PDF)

■ AUTHOR INFORMATION

Corresponding Authors

*E-mail: zhengzj@hubu.edu.cn.
*E-mail: zhanglq@mail.buct.edu.cn.
*E-mail: a.v.lyulin@tue.nl.

ORCID

Zijian Zheng: 0000-0001-5639-3841
Liqun Zhang: 0000-0002-8106-4721
Alexey V. Lyulin: 0000-0002-7533-3366

Notes

The authors declare no competing financial interest.

■ ACKNOWLEDGMENTS

This work is supported by the National Basic Research Program of China 2015CB654700(2015CB654704), the Foundation for Innovative Research Groups of the NSF of China (51221002), and the National Natural Science Foundation of China (51333004 and 51403015). The cloud calculation platform of BUCT is also greatly appreciated.

■ REFERENCES

(1) Crosby, A. J.; Lee, J. Y. Polymer Nanocomposites: The "Nano" Effect on Mechanical Properties. *Polym. Rev.* **2007**, *47*, 217−229.
(2) Tjong, S. C. Structural and Mechanical Properties of Polymer Nanocomposites. *Mater. Sci. Eng., R* **2006**, *53*, 73−197.
(3) Balazs, A. C.; Emrick, T.; Russell, T. P. Nanoparticle Polymer Composites: Where Two Small Worlds Meet. *Science* **2006**, *314*, 1107−1110.
(4) Srivastava, S.; Schaefer, J. L.; Yang, Z. C.; Tu, Z. Y.; Archer, L. A. 25th Anniversary Article: Polymer-Particle Composites: Phase Stability and Applications in Electrochemical Energy Storage. *Adv. Mater.* **2014**, *26*, 201−233.
(5) Jancar, J.; Douglas, J. F.; Starr, F. W.; Kumar, S. K.; Cassagnau, P.; Lesser, A. J.; Sternstein, S. S.; Buehler, M. J. Current Issues in Research on Structure-Property Relationships in Polymer Nanocomposites. *Polymer* **2010**, *51*, 3321−3343.
(6) Ganesan, V.; Jayaraman, A. Theory and Simulation Studies of Effective Interactions, Phase Behavior and Morphology in Polymer Nanocomposites. *Soft Matter* **2014**, *10*, 13−38.
(7) Moll, J. F.; Akcora, P.; Rungta, A.; Gong, S. S.; Colby, R. H.; Benicewicz, B. C.; Kumar, S. K. Mechanical Reinforcement in Polymer Melts Filled with Polymer Grafted Nanoparticles. *Macromolecules* **2011**, *44*, 7473−7477.
(8) Krishnamoorti, R.; Vaia, R. A. Polymer Nanocomposites. *J. Polym. Sci., Part B: Polym. Phys.* **2007**, *45*, 3252−3256.
(9) Yoffe, A. D. Semiconductor Quantum Dots and Related Systems: Electronic, Optical, Luminescence and Related Properties of Low Dimensional Systems. *Adv. Phys.* **2001**, *50*, 1−208.
(10) Moule, A. J.; Allard, S.; Kronenberg, N. M.; Tsami, A.; Scherf, U.; Meerholz, K. Effect of Polymer Nanoparticle Formation on the Efficiency of Polythiophene Based "Bulk-Heterojunction" Solar Cells. *J. Phys. Chem. C* **2008**, *112*, 12583−12589.
(11) Rolison, D. R.; Long, J. W.; Lytle, J. C.; Fischer, A. E.; Rhodes, C. P.; McEvoy, T. M.; Bourg, M. E.; Lubers, A. M. Multifunctional 3d Nanoarchitectures for Energy Storage and Conversion. *Chem. Soc. Rev.* **2009**, *38*, 226−252.
(12) Long, J. W.; Rolison, D. R. Architectural Design, Interior Decoration, and Three-Dimensional Plumbing En Route to Multifunctional Nanoarchitectures. *Acc. Chem. Res.* **2007**, *40*, 854−862.
(13) Bockstaller, M. R.; Thomas, E. L. Optical Properties of Polymer-Based Photonic Nanocomposite Materials. *J. Phys. Chem. B* **2003**, *107*, 10017−10024.
(14) Hore, M. J. A.; Composto, R. J. Nanorod Self-Assembly for Tuning Optical Absorption. *ACS Nano* **2010**, *4*, 6941−6949.
(15) Hore, M. J. A.; Composto, R. J. Using Miscible Polymer Blends to Control Depletion-Attraction Forces between Au Nanorods in Nanocomposite Films. *Macromolecules* **2012**, *45*, 6078−6086.
(16) Ferrier, R. C.; Lee, H. S.; Hore, M. J. A.; Caporizzo, M.; Eckmann, D. M.; Composto, R. J. Gold Nanorod Linking to Control Plasmonic Properties in Solution and Polymer Nanocomposites. *Langmuir* **2014**, *30*, 1906−1914.
(17) Moll, J.; Kumar, S. K.; Snijkers, F.; Vlassopoulos, D.; Rungta, A.; Benicewicz, B. C.; Gomez, E.; Ilavsky, J.; Colby, R. H. Dispersing Grafted Nanoparticle Assemblies into Polymer Melts through Flow Fields. *ACS Macro Lett.* **2013**, *2*, 1051−1055.
(18) Fernandes, N. J.; Koerner, H.; Giannelis, E. P.; Vaia, R. A. Hairy Nanoparticle Assemblies as One-Component Functional Polymer Nanocomposites: Opportunities and Challenges. *MRS Commun.* **2013**, *3*, 13−29.
(19) Ganesan, V.; Ellison, C. J.; Pryamitsyn, V. Mean-Field Models of Structure and Dispersion of Polymer-Nanoparticle Mixtures. *Soft Matter* **2010**, *6*, 4010−4025.
(20) Prolongo, S. G.; Meliton, B. G.; Del Rosario, G.; Urena, A. Simultaneous Dispersion and Alignment of Carbon Nanotubes in Epoxy Resin through Chronoamperometry. *Carbon* **2012**, *50*, 5489−5497.
(21) Mackay, M. E.; Tuteja, A.; Duxbury, P. M.; Hawker, C. J.; Van Horn, B.; Guan, Z. B.; Chen, G. H.; Krishnan, R. S. General Strategies for Nanoparticle Dispersion. *Science* **2006**, *311*, 1740−1743.
(22) Tuteja, A.; Duxbury, P. M.; Mackay, M. E. Polymer Chain Swelling Induced by Dispersed Nanoparticles. *Phys. Rev. Lett.* **2008**, DOI: 10.1103/PhysRevLett.100.077801.
(23) Pomposo, J. A.; de Luzuriaga, A. R.; Etxeberria, A.; Rodriguez, J. Key Role of Entropy in Nanoparticle Dispersion: Polystyrene-Nanoparticle/Linear-Polystyrene Nanocomposites as a Model System. *Phys. Chem. Chem. Phys.* **2008**, *10*, 650−651.
(24) Cai, X. X.; Li, B. P.; Pan, Y.; Wu, G. Z. Morphology Evolution of Immiscible Polymer Blends as Directed by Nanoparticle Self-Agglomeration. *Polymer* **2012**, *53*, 259−266.
(25) Krishnamoorti, R. Strategies for Dispersing Nanoparticles in Polymers. *MRS Bull.* **2007**, *32*, 341−347.
(26) Kasaliwal, G. R.; Goldel, A.; Potschke, P.; Heinrich, G. Influences of Polymer Matrix Melt Viscosity and Molecular Weight on Mwcnt Agglomerate Dispersion. *Polymer* **2011**, *52*, 1027−1036.
(27) Bar-Chaput, S.; Carrot, C. Rheology as a Tool for the Analysis of the Dispersion of Carbon Filler in Polymers. *Rheol. Acta* **2006**, *45*, 339−347.
(28) Khare, H. S.; Burris, D. L. A Quantitative Method for Measuring Nanocomposite Dispersion. *Polymer* **2010**, *51*, 719−729.
(29) Hooper, J. B.; Schweizer, K. S. Contact Aggregation, Bridging, and Steric Stabilization in Dense Polymer-Particle Mixtures. *Macromolecules* **2005**, *38*, 8858−8869.
(30) Shen, J. X.; Liu, J.; Gao, Y. Y.; Cao, D. P.; Zhang, L. Q. Revisiting the Dispersion Mechanism of Grafted Nanoparticles in Polymer Matrix: A Detailed Molecular Dynamics Simulation. *Langmuir* **2011**, *27*, 15213−15222.
(31) Zhang, Q.; Archer, L. A. Poly(Ethylene Oxide)/Silica Nanocomposites: Structure and Rheology. *Langmuir* **2002**, *18*, 10435−10442.
(32) Liu, L.; Sun, C. Z.; Li, Z. W.; Chen, Y. L.; Qian, X.; Wen, S. P.; Zhang, L. Q. In-Chain Functionalized Polymer Induced Assembly of Nanoparticles: Toward Materials with Tailored Properties. *Soft Matter* **2016**, *12*, 1964−1968.
(33) Chen, Y.; Chen, Q. Y.; Lv, Y. D.; Huang, Y. J.; Yang, Q.; Liao, X.; Niu, Y. H. Rheological Behaviors and Electrical Conductivity of

DOI: 10.1021/acs.jpcb.7b08670
J. Phys. Chem. B 2017, 121, 9311−9318

Long-Chain Branched Polypropylene/Carbon Black Composites with Different Methods. *J. Polym. Res.* **2015**, DOI: 10.1007/s10965-015-0751-1.
(34) Liu, D.; Pourrahimi, A. M.; Olsson, R. T.; Hedenqvist, M. S.; Gedde, U. W. Influence of Nanoparticle Surface Treatment on Particle Dispersion and Interfacial Adhesion in Low-Density Polyethylene/Aluminium Oxide Nanocomposites. *Eur. Polym. J.* **2015**, *66*, 67−77.
(35) Sliozberg, Y. R.; Chantawansri, T. L.; Lenhart, J. L.; Andzelm, J. W. Structural and Mechanical Properties of Advanced Polymer Gels with Rigid Side-Chains Using Coarse-Grained Molecular Dynamics. *Polymer* **2014**, *55*, 5266−5275.
(36) Bockstaller, M. R.; Mickiewicz, R. A.; Thomas, E. L. Block Copolymer Nanocomposites: Perspectives for Tailored Functional Materials. *Adv. Mater.* **2005**, *17*, 1331−1349.
(37) Jouault, N.; Lee, D.; Zhao, D.; Kumar, S. K. Block-Copolymer-Mediated Nanoparticle Dispersion and Assembly in Polymer Nanocomposites. *Adv. Mater.* **2014**, *26*, 4031−4036.
(38) Vaia, R. A.; Maguire, J. F. Polymer Nanocomposites with Prescribed Morphology: Going Beyond Nanoparticle-Filled Polymers. *Chem. Mater.* **2007**, *19*, 2736−2751.
(39) Fazli, Y.; Kulani, E.; Khezri, K.; Alijani, H. Pmma-Grafted Silica Aerogel Nanoparticles Via in Situ Sr&Ni Atrp: Grafting through Approach. *Microporous Mesoporous Mater.* **2015**, *214*, 70−79.
(40) Gambinossi, F.; Mylon, S. E.; Ferri, J. K. Aggregation Kinetics and Colloidal Stability of Functionalized Nanoparticles. *Adv. Colloid Interface Sci.* **2015**, *222*, 332−349.
(41) Ku, K. H.; Yang, H.; Shin, J. M.; Kim, B. J. Aspect Ratio Effect of Nanorod Surfactants on the Shape and Internal Morphology of Block Copolymer Particles. *J. Polym. Sci., Part A: Polym. Chem.* **2015**, *53*, 188−192.
(42) Estridge, C. E.; Jayaraman, A. Effect of Homopolymer Matrix on Diblock Copolymer Grafted Nanoparticle Conformation and Potential of Mean Force: A Molecular Simulation Study. *J. Polym. Sci., Part B: Polym. Phys.* **2015**, *53*, 76−88.
(43) Hauser, A. W.; Hayward, R. C. Random Photografting of Polymers to Nanoparticles for Well-Dispersed Nanocomposites. *J. Polym. Sci., Part B: Polym. Phys.* **2016**, *54*, 152−158.
(44) Jiao, Y.; Akcora, P. Understanding the Role of Grafted Polystyrene Chain Conformation in Assembly of Magnetic Nanoparticles. *Phys. Rev. E* **2014**, DOI: 10.1103/PhysRevE.90.042601.
(45) Kremer, K.; Grest, G. S. Dynamics of Entangled Linear Polymer Melts: A Molecular-Dynamics Simulation. *J. Chem. Phys.* **1990**, *92*, 5057−5086.
(46) Morris, D.; Morriss, G. *Statistical Mechanics of Nonequilibrium Liquids*; Academic Press: London, 1990; Chapter 6.
(47) Toepperwein, G. N.; de Pablo, J. J. Cavitation and Crazing in Rod-Containing Nanocomposites. *Macromolecules* **2011**, *44*, 5498−5509.
(48) Liu, J.; Shen, J.; Zheng, Z.; Wu, Y.; Zhang, L. Revealing the Toughening Mechanism of Graphene−Polymer Nanocomposite through Molecular Dynamics Simulation. *Nanotechnology* **2015**, *26*, 291003.
(49) Gao, J.; Weiner, J. Simulated Polymer Melt Stress Relaxation. I. Plateau Behavior. *J. Chem. Phys.* **1995**, *103*, 1614−1620.
(50) Gao, J.; Weiner, J. H. Bond Orientation Decay and Stress Relaxation in a Model Polymer Melt. *Macromolecules* **1996**, *29*, 6048−6055.
(51) Plimpton, S. Fast Parallel Algorithms for Short-Range Molecular Dynamics. *J. Comput. Phys.* **1995**, *117*, 1−19.
(52) Zheng, Z.; Liu, H.; Shen, J.; Liu, J.; Wu, Y.; Zhang, L. Tailoring the Static and Dynamic Mechanical Properties of Tri-Block Copolymers through Molecular Dynamics Simulation. *Polymers* **2016**, *8*, 335.
(53) Zheng, Z.; Shen, J.; Liu, J.; Wu, Y.; Zhang, L.; Wang, W. Tuning the Visco-Elasticity of Elastomeric Polymer Materials Via Flexible Nanoparticles: Insights from Molecular Dynamics Simulation. *RSC Adv.* **2016**, *6*, 28666−28678.
(54) Liu, J.; Zhang, L.; Cao, D.; Shen, J.; Gao, Y. Computational Simulation of Elastomer Nanocomposites: Current Progress and Future Challenges. *Rubber Chem. Technol.* **2012**, *85*, 450−481.
(55) Wang, M.-J.; Wolff, S. Filler-Elastomer Interactions. Part V. Investigation of the Surface Energies of Silane-Modified Silicas. *Rubber Chem. Technol.* **1992**, *65*, 715−735.
(56) Wang, Z.; Zheng, Z.; Liu, J.; Wu, Y.; Zhang, L. Tuning the Mechanical Properties of Polymer Nanocomposites Filled with Grafted Nanoparticles by Varying the Grafted Chain Length and Flexibility. *Polymers* **2016**, *8*, 270.

DOI: 10.1021/acs.jpcb.7b08670
J. Phys. Chem. B 2017, 121, 9311−9318